

CDMA/OTFS Sensing Outperforms Pure OTFS at the Same Communication Throughput

HUGO HAWKINS*, GRADUATE STUDENT MEMBER, IEEE, CHAO XU*, SENIOR MEMBER, IEEE, LIE-LIANG YANG*, FELLOW, IEEE, AND LAJOS HANZO*, LIFE FELLOW, IEEE

¹School of Electronics and Computer Science, University of Southampton, Southampton SO17 1BJ, UK

CORRESPONDING AUTHOR: Lajos Hanzo (e-mail: lh@ecs.soton.ac.uk).

L. Hanzo would like to acknowledge the financial support of the Engineering and Physical Sciences Research Council (EPSRC) projects under grant EP/Y037243/1, EP/W016605/1, EP/X01228X/1, EP/Y026721/1, EP/W032635/1, EP/Y037243/1 and EP/X04047X/1 as well as of the European Research Council's Advanced Fellow Grant QuantCom (Grant No. 789028).

ABSTRACT There is a dearth of publications on the subject of spreading-aided Orthogonal Time Frequency Space (OTFS) solutions, especially for Integrated Sensing and Communication (ISAC), even though Code Division Multiple Access (CDMA) assisted multi-user OTFS (CDMA/OTFS) exhibits tangible benefits. Hence, this work characterises both the communication Bit Error Rate (BER) and sensing Root Mean Square Error (RMSE) performance of CDMA/OTFS, and contrasts them to pure OTFS.

Three CDMA/OTFS configurations are considered: Delay Code Division Multiple Access OTFS (DI-CDMA/OTFS), Doppler Code Division Multiple Access OTFS (Dp-CDMA/OTFS), and Delay Doppler Code Division Multiple Access OTFS (DD-CDMA/OTFS), which harness direct sequence spreading along the delay axis, Doppler axis, and DD domains respectively. For each configuration, the performance of Gold, Hadamard, and Zadoff-Chu sequences is investigated.

The results demonstrate that Zadoff-Chu DI-CDMA/OTFS and DD-CDMA/OTFS consistently outperform pure OTFS sensing, whilst maintaining a similar communication performance at the same throughput. The extra modulation complexity of CDMA/OTFS is similar to that of other OTFS multi-user methodologies, but the demodulation complexity of CDMA/OTFS is lower than that of some other OTFS multi-user methodologies. CDMA/OTFS sensing can also consistently outperform OTFS sensing whilst not requiring any additional complexity for target parameter estimation. Therefore, CDMA/OTFS is an appealing candidate for implementing multi-user OTFS ISAC.

INDEX TERMS Code Division Multiple Access, Integrated Sensing and Communication, Orthogonal Time Frequency Space, Sequence Spreading

I. INTRODUCTION

INTEGRATED Sensing and Communication (ISAC) is a subject of considerable interest for future wireless generations [1]–[4], as the number of wireless devices is expected to drastically increase. Since the OTFS concept was first introduced [5], [6], its employment for ISAC [7] has been a topic of interest. This is due in part to OTFS being less affected by Doppler shift than Orthogonal Frequency-Division Multiplexing (OFDM), and to the DD channel being defined by the delay and Doppler shifts of the propagation

paths. This leads to the DD channel fluctuating at a slower rate than its Time Frequency Domain (TFD) and Time Domain (TD) counterparts. When the delay and Doppler shifts of the propagation paths are perfectly synchronous with the system's sampling grid, the channel can be modelled using a sparse matrix. This can simplify the associated target parameter estimation algorithms [8].

However, in practice, the delay and Doppler shifts are rarely integer multiples of the system resolutions, hence more complex detection algorithms are required for accurate

target estimation. The full-search based Maximum Likelihood (ML) attains the best performance at the highest complexity. Hence, Gaudio *et al.* [9] compare the sensing performance of OFDM and OTFS employing ML detection applied to the entire possible set of delay and Doppler indices, at an unspecified resolution. At low velocities, where the Doppler shift is 0.28% of the subcarrier spacing, OFDM ML sensing approaches the Cramér-Rao Bound (CRB) at a lower Signal to Noise Ratio (SNR) than OTFS. This suggests that at low velocities, OFDM is more suitable for sensing than OTFS. However, [9] does not compare the two waveforms at high velocities.

In [10], [11], the authors conceive a two dimensional correlation-based method for OTFS integer delay and Doppler index estimation. A generalised likelihood ratio test is developed to estimate the number of targets. The fractional indices of the estimated targets are determined by comparing the power-ratio of the indices surrounding the estimated integer indices in the imaging matrix. This method requires each target to have unique integer delay and Doppler indices. The authors observe that the correlation-based method results in an error floor at high SNRs due to the inter-symbol interference caused by the multiple propagation paths in the channel. Tang *et al.* [12] propose a two-step sensing methodology to estimate the integer and fractional delay and Doppler indices of the targets for OTFS sensing. The first step employs a matched filter-based method to determine the integer indices. The second step utilises a Fibonacci-search based algorithm to iteratively determine the fractional indices. Unlike other parameter estimation methods, which reach an error floor at high SNRs, the estimation error of the Fibonacci-search based algorithm continues to decrease as the SNR increases.

In [13], Muppaneni *et al.* design a two-step method for sensing the target parameters of OTFS. Firstly, the integer indices are estimated by maximising a cost function for a fixed number of propagation paths. Secondly, the fractional indices are estimated using a matrix of all the integer indices and the previously estimated fractional indices. For the first path, only integer indices of the other paths are utilised to estimate the first path fractional indices. Once the fractional indices for a path have been estimated, the channel attenuation of the associated path is then estimated. After the fractional indices of a path are estimated, the difference between the received signal and the reconstructed received signal from the estimates is calculated. If this difference becomes smaller than a specific threshold, the sensing procedure is terminated, and path estimation is concluded. Otherwise, the algorithm continues until the fixed number of propagation path variables has been estimated. This method is also harnessed for communication channel estimation using pilot frames. The results presented in [13] show that the proposed algorithm leads to a lower sensing estimation error and communication BER than the modified ML benchmark used for comparison.

A low-complexity variant of OTFS, known as Orthogonal Time Sequency Multiplexing (OTSM), was first introduced by Thaj *et al.* [14]. This waveform modulates the symbols in the delay-sequency (sic) domain, as opposed to the DD of OTFS. This is achieved by replacing the Inverse Discrete Fourier Transform (IDFT) along the Doppler axis by the Walsh-Hadamard transform. Since this is a purely real-valued transform, a real-valued transmitted signal can be generated by employing a real-valued modulation scheme. The Hadamard transform is also more computationally efficient than the Discrete Fourier Transform (DFT) and the IDFT used for OTFS. However, since the modulated waveform is constructed in the delay-sequency domain, not the DD, the propagation paths with identical delays cannot be separated without more complex detection methods, even if they have different Doppler shifts. Thaj *et al.* [14] show that OTSM has a similar BER performance to OTFS, but it is computationally more efficient due to the use of the Hadamard transform. The pilot power and Peak to Average Power Ratio (PAPR) of OTSM is reduced by Neelam and Sahuin [15], by superimposing the pilot symbols on the data, and employing a low complexity iterative channel estimator. Moreover, the BER upper bound of OTSM is determined by Sui *et al.* [16], and a novel vector approximate message passing-based expectation-maximization detector is developed to improve the BER performance of OTSM.

Doosti-Aref *et al.* [17] harness Index Modulation (IM) in the sequency domain, to improve both the spectral efficiency and BER of OTSM. This method is further developed in [18], where pairs of sequence indices of the sequency domain are determined by IM, as opposed to detecting individual indices. This improves the energy efficiency of the system, and reduces the error propagation imposed by erroneous activated index estimation.

The estimation and compensation of the In-phase and Quadrature-phase (IQ) imbalance in the received signal caused by the hardware at high frequencies is investigated for OTSM and OTFS by Neelam and Sahu [19]. The estimation is achieved by placing two pilot symbols in the delay-sequency domain transmitted signal, and then estimating the imbalance based on these symbols in the delay-time domain. The addition of a second pilot symbol decreases the number of indices available for data, since guard bands are also required between the pilot symbols, in addition to the guard band between the pilot symbols and the data. The IQ compensation is implemented in the delay-time domain. The compensation of the imbalance is improved as the pilot power is increased. This work is then also extended to determine both the carrier frequency offset and the channel parameters by Neelam and Sahu [20], where both integer delay and fractional Doppler indices are considered.

The work in [19] is further extended to transmitter and receiver imbalance estimation and compensation as well as channel estimation by the same authors [21]. A complex pseudo noise-based training sequence is placed in the indices

allocated to the pilot symbols. The imaginary part of the sequence is a cyclic shift of the real part of the sequence. The channel is estimated at discrete intervals, where the initial estimations are further refined by linear interpolation. An iterative algorithm is conceived for estimating and compensating the IQ imbalance.

Singh et al. [22] implement a deep learning-based detector for OTSM to compensate for hardware impairments. This deep learning-based detector involves a convolutional neural network, which is trained on the transmitted, received, and Minimum Mean Square Error (MMSE) detector outputs. A data augmentation scheme is then developed to further enhance the input data to the neural network. The resultant detector has a slightly higher complexity than an MMSE detector, whilst reducing the BER.

Reddy et al. [23] design a multi-user uplink method based on upsampled and circularly shifted OFDM. These signals, when combined at the base station, are equivalent to single-user OTFS, OTSM, or block-based single carrier signals. This is equivalent to a system that allocates delay indices to users, where the secondary domain of the data can be selected simply by interchanging the matrix multiplying the modulated data. Specifically, the system may opt for the IDFT for OTFS/Zak-OTFS, the Hadamard transform for OTSM, or the identity matrix for single carrier TD schemes. The BER performance of the OTSM method is comparable to that of the OTFS method.

Another method applying a real-valued transform to OTFS is proposed by Kalpage et al. [24]. A modified Zak-OTFS method relying on the Discrete Cosine Transform (DCT) is developed to reduce the PAPR of OTFS. Replacing the DFT by the DCT reduces both the PAPR and the complexity of the system, without eroding the BER for the conditions considered by the authors.

Surabhi et al. [25] design a multi-user OTFS system that splits the available DD indices into multiple sub-groups, each of which is allocated to a user. The sub-groups can be along the delay axis, the Doppler axis, or both axes. The BER of the schemes relying on index groups along the delay or Doppler axis is lower than that of the schemes that allocate indices for a user along two axes. The BER of this system using ML or message passing-based detection is lower than that of Orthogonal Frequency-Division Multiple Access (OFDMA) and Single Carrier Frequency-Division Multiple Access (SC-FDMA).

Khammammetti and Mohammed [26] propose a DD index allocation method for multi-user communications similar to that of [25], but place guard bands between the indices assigned to users, to minimise the inter-user interference. This leads to a simpler detector, at the cost of an eroded throughput.

Ge et al. [27] apply the DD matrix partitioning method to uplink communication, separating stationary and mobile devices. The stationary devices modulate along the delay axis, and the mobile devices modulate along the Doppler

axis. As the base station is static, the stationary users do not experience Doppler shift. A successive interference cancellation aided iterative turbo receiver utilising soft inputs and outputs is developed for detecting the uplink signals. The stationary user signals are decoded, followed by the information arriving from the mobile devices.

Sparse Code Multiple Access (SCMA) has been amalgamated in conjunction with OTFS in [29]–[31], [34], relying on Non-Orthogonal Multiple Access (NOMA) for supporting a higher number of users than the number of available resources blocks, albeit at the cost of increased inter-user interference.

Thomas et al. [29] allocate the modulated symbols along either the delay or Doppler axes using sparse codes. Both the uplink and downlink are considered. In the downlink, a single pilot symbol associated with an appropriate guard band is used for channel estimation, to achieve a communication performance close to the perfect channel estimation case. For the uplink, a sophisticated channel estimation method is developed without excessive guard band overhead, as the effect of the sparse codes on the symbols cannot be separated from the multipath channel effects. Convolutional sparse coding techniques are utilised for uplink channel estimation, as the pilot symbols also rely on sparse codes in the pilot band, surrounded by guard bands.

Wen et al. [31], [34] allocate the symbols based on each user's sparse code along the delay and Doppler indices. The system firstly estimates the vector of superimposed transmitted symbols from all users in the TD, then decodes the symbols gleaned from each user in the DD employing a message passing algorithm. The system iterates between the two domains to accurately estimate the transmitted symbols.

Deka et al. [30] harness SCMA OTFS for both uplink and downlink communication, with the sparse codes aligned either along the delay axis, or the Doppler axis. Channel estimation is performed by embedding a pilot symbol surrounded by guard bands in the transmitted signal. The results show a lower BER for SCMA OTFS than for power-domain OTFS NOMA and DD index allocation OTFS for the same normalised user load.

Although SCMA-OTFS is a promising multi-user method, the characteristics of the transmitted signal are not optimal for sensing, since signals exhibiting a higher degree of randomness lead to an eroded sensing performance [35]. The sparsity of the codes is beneficial for reducing the detection and demodulation complexity, but increases the signal variability. This issue is also observed when IM is harnessed [36].

There are also a few publications on dense sequence spreading OTFS [28], [32], [33]. In [32], Sun et al. spread the symbols along the delay axis of the DD matrix. Two spreading sequence methods are considered: a single spreading sequence used to spread each symbol, or separate sequences used to spread each symbol. In the first case, a sequence having good autocorrelation properties is designed. In the

TABLE 1: Contrasting contributions to the literature

Papers Topics	[28]	[29]	[30]	[31]	[23]	[25]	[32]	[33]	[34]	This work
Channel modeling										
Fractional delay indices										✓
Fractional Doppler indices			✓	✓		✓			✓	✓
Sequence spreading										
Sequence spreading	✓	✓	✓	✓	✓		✓	✓	✓	✓
Dense sequences ¹	✓				✓		✓	✓		✓
Multi-user methods										
Multi-user communication	✓	✓	✓	✓	✓	✓			✓	✓
Resource allocation on delay only	✓	✓	✓			✓	✓			✓
Resource allocation on Doppler only		✓	✓			✓		✓		✓
Resource allocation on DD indices				✓		✓			✓	✓
Code multiple access methods	✓	✓	✓	✓					✓	✓
Code multiple access along the delay only, Doppler only, and DD indices										✓
ISAC										
Code multiple access OTFS communication and sensing										✓
Effect of spreading on the sensing RMSE performance										✓

¹ Dense sequences: all or the majority of the elements have a non-zero value, as opposed to sparse sequences

second case, the optimisation problem is too complex, due to the immense variety of possible sequence combinations. Gold and m -sequences are used in this case. The BER of spread OTFS is shown to be lower than that of Direct Sequence Spread Spectrum (DSSS) or spread OFDM.

In Cao et al. [33], each symbol is spread along the Doppler axis using m -sequences. A rake receiver is designed to detect the symbols. The channel is assumed to have two paths, each with identical delays. This novel receiver leads to a lower BER than conventional MMSE detection in the limited channel conditions considered. The performance difference is more pronounced if the gains of each path are of similar magnitude.

In Ma et al. [28], the users are assigned to groups. Each user group is allocated a Doppler index, with each user symbol spread over the delay indices at the user group Doppler index. The sequences utilised are cyclically orthogonal, such as the columns or rows of a DFT matrix. The spread symbols are interleaved along the delay axis. However, no performance comparison to OTFS is provided.

A. Contributions

Again, there is a paucity of publications on the subject of dense sequence spreading OTFS, especially for ISAC. Hence, this work analyses the communication BER and sensing RMSE performance of CDMA/OTFS, and contrasts them with pure OTFS. Table 1 explicitly juxtaposes the novelties of the proposed system to the existing literature, which are detailed below:

TABLE 2: Notations

Definition	Example	Description
Scalar value	a/A	Italics
Vector	\mathbf{a}	Bold lower case
Matrix	\mathbf{A}	Bold upper case
Vector or matrix transpose	$(\cdot)^T$	
Complex conjugate operation	$(\cdot)^*$	
Complex conjugate transpose	$(\cdot)^H$	
Inverse of a matrix	$(\cdot)^{-1}$	

- A detailed analysis of CDMA/OTFS in the context of ISAC is provided, where both fractional delay indices and fractional Doppler indices are considered.
- An in-depth analysis of the communication BER and sensing RMSE performance of delay only, Doppler only, and delay-Doppler sequence spreading for CDMA/OTFS.
- This work demonstrates that Zadoff-Chu DL-CDMA/OTFS and DD-CDMA/OTFS are the configurations that consistently outperform pure OTFS sensing, whilst maintaining a similar communication performance at the same throughput.

The notations used are shown in Table 2.

II. Transmit Signal Model

Sequence spreading across the delay, Doppler, or delay and Doppler indices is applied to OTFS, relying on Gold, Hadamard, and Zadoff-Chu sequences. A sequence of length M is used for delay-domain spreading, of length N for

Doppler-domain spreading, and of length MN for DD spreading, where M is the number of subcarriers, and N is the number of symbols slots.

Each sequence \mathbf{c} is power-normalised, hence:

$$\mathbf{c}^H \mathbf{c} = 1, \quad (1)$$

where $(\cdot)^H$ is the Hermitian/complex transpose.

The matrix \mathbf{C} containing all of the spreading sequences utilised is:

$$\mathbf{C} = (\mathbf{c}_0, \mathbf{c}_1, \dots, \mathbf{c}_{N_{mult}-1}), \quad (2)$$

where N_{mult} is the number of multiplexed modulated sequences.

The DD transmitted signal vector $\tilde{\mathbf{x}} \in \mathbb{C}^{MN \times 1}$ is expressed as:

$$\tilde{\mathbf{x}} = \mathfrak{C} \mathbf{s}, \quad (3)$$

where $\mathbf{s} \in \mathbb{C}^{N_s \times 1}$ is the vector of the modulated symbols, $\mathfrak{C} \in \mathbb{C}^{MN \times N_s}$ is the spreading matrix containing the spreading sequences, where the arrangement of the sequences is dependent on the specific CDMA/OTFS scheme implemented. Furthermore, N_s denotes the number of symbols transmitted in a frame. The system throughput is $\frac{\beta N_s}{MN}$ Bits Per Channel Use (bpcu), where β is the number of bits per symbol. The Cyclic Prefix (CP) is assumed to be sufficiently long, and it is perfectly removed from the received signal at the receiver.

A. Delay Code Division Multiple Access OTFS

For DI-CDMA/OTFS, each modulated symbol $s_{n_{mult}, n}$ is multiplied by a spreading sequence $\mathbf{c}_{n_{mult}} \in \mathbb{C}^{M \times 1}$, where $n_{mult} = (0, 1, \dots, N_{mult} - 1)$, and $n = (0, 1, \dots, N - 1)$. The total number of transmitted symbols $N_s = N_{mult}N$, and the maximum number of multiplexed sequences is M , hence $1 \leq N_{mult} \leq M$.

The DD transmitted signal matrix representation $\tilde{\mathbf{X}} \in \mathbb{C}^{M \times N}$ is:

$$\tilde{\mathbf{X}} = \mathbf{C} \mathbf{S}, \quad (4)$$

where $\mathbf{C} \in \mathbb{C}^{M \times N_{mult}}$, $\mathbf{S} \in \mathbb{C}^{N_{mult} \times N}$, and $\mathbf{S}[n_{mult}, n] = s_{n_{mult}, n}$.

The columns of $\tilde{\mathbf{X}}$ are stacked to create the DD transmitted signal vector $\tilde{\mathbf{x}}$:

$$\tilde{\mathbf{x}}[nM : (n+1)M - 1] = \tilde{\mathbf{X}}[0 : M - 1, n], \quad (5)$$

where $n = (0, 1, \dots, N - 1)$.

The symbols can also be directly spread to form $\tilde{\mathbf{x}}$, as in (3), where:

$$\mathbf{s}[nN_{mult} + n_{mult}] = s_{n_{mult}, n}, \quad (6)$$

$$\mathfrak{C} = \text{diag}(\mathbf{C}), \quad (7)$$

and $\text{diag}(\mathbf{C})$ is the diagonal operator, which creates a matrix whose diagonal elements are \mathbf{C} .

As an example, for $M = 4$, $N = 3$, $N_{mult} = 2$, $\mathbf{C} \in \mathbb{C}^{M \times N_{mult}} = \mathbb{C}^{4 \times 2}$, and \mathfrak{C} is:

$$\mathfrak{C} = \begin{bmatrix} \mathbf{C} & \mathbf{0}_{4 \times 2} & \mathbf{0}_{4 \times 2} \\ \mathbf{0}_{4 \times 2} & \mathbf{C} & \mathbf{0}_{4 \times 2} \\ \mathbf{0}_{4 \times 2} & \mathbf{0}_{4 \times 2} & \mathbf{C} \end{bmatrix}, \quad (8)$$

where $\mathbf{0}_{4 \times 2}$ is a 4×2 matrix of 0.

B. Doppler Code Division Multiple Access OTFS

For Dp-CDMA/OTFS, each modulated symbol $s_{m, n_{mult}}$ is multiplied by a spreading sequence $\mathbf{c}_{n_{mult}} \in \mathbb{C}^{N \times 1}$, where $m = (0, 1, \dots, M - 1)$. The total number of transmitted symbols is $N_s = N_{mult}M$, and the maximum number of multiplexed sequences is N , hence $1 \leq N_{mult} \leq N$.

The DD transmitted signal matrix representation $\tilde{\mathbf{X}}$ is:

$$\tilde{\mathbf{X}} = \mathbf{S} \mathbf{C}^T, \quad (9)$$

where $(\cdot)^T$ is the transpose operation, $\mathbf{C} \in \mathbb{C}^{N \times N_{mult}}$, $\mathbf{S} \in \mathbb{C}^{M \times N_{mult}}$, $\mathbf{S}[m, n_{mult}] = s_{m, n_{mult}}$, and $m = (0, 1, \dots, M - 1)$.

The columns of $\tilde{\mathbf{X}}$ are stacked to create the DD transmitted signal vector $\tilde{\mathbf{x}}$, as shown in (5). The symbols can also be directly spread to form $\tilde{\mathbf{x}}$, as in (3), where:

$$\mathbf{s}[mN_{mult} + n_{mult}] = s_{m, n_{mult}}, \quad (10)$$

$$\mathfrak{C}[nM + m, mN_{mult} : (m+1)N_{mult} - 1] = \mathbf{C}[n, 0 : N_{mult} - 1], \quad (11)$$

with $m = (0, 1, \dots, M - 1)$, and $n = (0, 1, \dots, N - 1)$.

As an example, for $M = 4$, $N = 3$, $N_{mult} = 2$, $\mathbf{C} \in \mathbb{C}^{N \times N_{mult}} = \mathbb{C}^{3 \times 2}$, and \mathfrak{C} is as shown in (12).

C. Delay Doppler Code Division Multiple Access OTFS

For DD-CDMA/OTFS, each modulated symbol $s_{n_{mult}}$ is multiplied by a spreading sequence $\mathbf{c}_{n_{mult}} \in \mathbb{C}^{MN \times 1}$. The total number of transmitted symbols $N_s = N_{mult}$, and the maximum number of multiplexed sequences is MN , hence $1 \leq N_{mult} \leq MN$. The DD-CDMA/OTFS scheme can therefore support more users by relying on a greater number of unique spreading sequences than DI-CDMA/OTFS and Dp-CDMA/OTFS.

The symbols are directly spread to form $\tilde{\mathbf{x}}$, as in (3):

$$\tilde{\mathbf{x}} = \sum_{n_{mult}=0}^{N_{mult}-1} \mathbf{c}_{n_{mult}} s_{n_{mult}} = \mathbf{C} \mathbf{s}, \quad (13)$$

where $\mathbf{s} \in \mathbb{C}^{N_{mult}}$, $\mathbf{C} \in \mathbb{C}^{MN \times N_{mult}}$, and $\mathfrak{C} = \mathbf{C}$.

III. Channel Model

In this section, the channel models are introduced. The generalised TD, TFD, and DD channel models are described in Section A. The communication channel parameters are presented in Section B, while the sensing channel parameters are discussed in Section C.

A. Generalised Channel Model

It is assumed that there is no external interference during transmission. The transmitted signal is passed through a time-varying and frequency-selective fading channel, as modelled in [37]. The DD representation of the fading channel is:

$$\tilde{h}(\tau, \nu) = \sum_{p=0}^{P-1} \tilde{h}_p \delta(\tau - \tau_p) \delta(\nu - \nu_p), \quad (14)$$

where τ is the delay, ν is the Doppler shift, $p = [0, 1, \dots, P-1]$ is the propagation path index, and P is the total number of propagation paths. Furthermore, τ_p is the delay associated with the p^{th} path, ν_p is the Doppler shift associated with the p^{th} path, \tilde{h}_p is the fading gain and path loss associated with the p^{th} path, and $\delta(\cdot)$ is the Dirac delta function.

When sampled in the DD, the channel can be represented by the time-invariant parameter \tilde{h}_p , the delay index τ^i , and the Doppler index ν^i . The delay and Doppler indices are defined as:

$$\tau^i = (\Delta f M) \tau, \quad (15)$$

$$\nu^i = \frac{N}{\Delta f} \nu, \quad (16)$$

where Δf is the subcarrier spacing.

The TD representation of the fading channel is:

$$h_{m,n,p} = \tilde{h}_p e^{j2\pi \nu_p^i \frac{nM+m-\tau_p^i}{MN}}, \quad (17)$$

where $j = \sqrt{-1}$, τ_p^i is the delay index associated with the p^{th} propagation path, and ν_p^i is the Doppler index associated with the p^{th} propagation path.

The TD channel matrix $\mathbf{H}_n \in \mathbb{C}^{M \times M}$ is:

$$\mathbf{H}_n[m, [m - \tau_p^i]_M] = \sum_{p=0}^{P-1} h_{m,n,p}, \quad (18)$$

where $[\cdot]_M$ is the modulo M operator.

When the delay indices are assumed to be integers, the TD received signal $\mathbf{y} \in \mathbb{C}^{M \times 1}$ is

$$\mathbf{y}_n = \mathbf{H}_n \mathbf{x}_n + \mathbf{z}, \quad (19)$$

where $\mathbf{x}_n \in \mathbb{C}^{M \times 1}$ is the TD transmitted signal, and \mathbf{z} is the complex TD Additive White Gaussian Noise (AWGN), with mean $\mu_z = 0$ and variance σ_z^2 , expressed as $\mathcal{N}(\mu_z, \sigma_z^2)$.

When the integer delay index assumption is discarded, $(m - \tau_p^i)$ is not an integer for $m = (0, 1, \dots, M-1)$. As matrices do not have fractional indices, the channel must be modelled differently. A portion of the fading channel is modelled in the TFD and then converted to the TD as

follows:

$$\mathbf{y}_n[m] = \frac{1}{\sqrt{M}} \sum_{p=0}^{P-1} h_{m,n,p} \sum_{\bar{m}=0}^{M-1} \bar{\mathbf{x}}_n[\bar{m}] e^{j2\pi \frac{(m-\tau_p^i)\bar{m}}{M}} + \mathbf{z}_n[m], \quad (20)$$

where $\bar{\mathbf{x}} \in \mathbb{C}^{M \times N}$ is the TFD transmitted signal, and $\bar{m} = [0, 1, \dots, M-1]$.

The TFD channel matrix $\bar{\mathbf{H}}_n \in \mathbb{C}^{M \times M}$ is:

$$\bar{\mathbf{H}}_n = \mathcal{F}_M \mathbf{H}_n \mathcal{F}_M^H, \quad (21)$$

where \mathcal{F}_M is the M -point DFT and \mathcal{F}_M^H is the M -point IDFT.

The DD channel matrix $\tilde{\mathbf{H}} \in \mathbb{C}^{MN \times MN}$ is:

$$\tilde{\mathbf{H}} = (\mathcal{F}_N \otimes \mathcal{F}_M^H) \bar{\mathbf{H}}_X (\mathcal{F}_N^H \otimes \mathcal{F}_M), \quad (22)$$

where \otimes is the Kronecker product, and

$$\bar{\mathbf{H}}_X = \text{diag}(\bar{\mathbf{H}}_n) = \begin{bmatrix} \bar{\mathbf{H}}_0 & \mathbf{0}_{M \times M} & \cdots & \mathbf{0}_{M \times M} \\ \mathbf{0}_{M \times M} & \bar{\mathbf{H}}_1 & \cdots & \mathbf{0}_{M \times M} \\ \vdots & \vdots & \ddots & \vdots \\ \mathbf{0}_{M \times M} & \mathbf{0}_{M \times M} & \cdots & \bar{\mathbf{H}}_{N-1} \end{bmatrix}. \quad (23)$$

B. Communication Channel Parameters

Integer delay indices, fractional Doppler indices, and Rician fading are assumed for communication. There are P_{com} propagation paths. The first path $p_{com} = 0$ is the Line of Sight (LoS) path, and the remaining $P_{com} - 1$ paths are Non-Line of Sight (NLoS) paths. The fading gain $\tilde{h}_{p,com}$ of the p_{com}^{th} propagation path is:

$$\tilde{h}_{p,com} = \begin{cases} \sqrt{\frac{\kappa_{com}}{\kappa_{com}+1}}, & \text{if } p_{com} = 0 \\ \sqrt{\frac{1}{(\kappa_{com}+1)(P_{com}-1)}} \zeta_{p,com}, & \text{if } p_{com} > 0, \end{cases} \quad (24)$$

where κ_{com} is the Rician K factor, and $\zeta_{p,com}$ is a complex Gaussian random variable with mean $\mu_{com} = 0$ and variance $\sigma_{com}^2 = 1$, expressed as $\mathcal{N}(\mu_{com}, \sigma_{com}^2)$.

$$\mathbf{c} = \begin{bmatrix} C[0,0] & C[0,1] & 0 & 0 & 0 & 0 & 0 & 0 \\ 0 & 0 & C[0,0] & C[0,1] & 0 & 0 & 0 & 0 \\ 0 & 0 & 0 & 0 & C[0,0] & C[0,1] & 0 & 0 \\ 0 & 0 & 0 & 0 & 0 & 0 & C[0,0] & C[0,1] \\ C[1,0] & C[1,1] & 0 & 0 & 0 & 0 & 0 & 0 \\ 0 & 0 & C[1,0] & C[1,1] & 0 & 0 & 0 & 0 \\ 0 & 0 & 0 & 0 & C[1,0] & C[1,1] & 0 & 0 \\ 0 & 0 & 0 & 0 & 0 & 0 & C[1,0] & C[1,1] \\ C[2,0] & C[2,1] & 0 & 0 & 0 & 0 & 0 & 0 \\ 0 & 0 & C[2,0] & C[2,1] & 0 & 0 & 0 & 0 \\ 0 & 0 & 0 & 0 & C[2,0] & C[2,1] & 0 & 0 \\ 0 & 0 & 0 & 0 & 0 & 0 & C[2,0] & C[2,1] \end{bmatrix}. \quad (12)$$

The integer delay index $\tau_{p,com}^i$ is:

$$\tau_{p,com}^i = \begin{cases} 0, & \text{if } p_{com} = 0 \\ p_{com} \% L_{com}, & \text{if } p_{com} > 0 \ \& \ P_{com} \geq L_{com} \\ \lfloor L_{com} \eta_{\tau,com} \rfloor, & \text{if } p_{com} > 0 \ \& \ P_{com} < L_{com}, \end{cases} \quad (25)$$

where L_{com} is the number of delay taps, $p_{com} = [0, 1, \dots, P_{com} - 1]$, $\%$ is the remainder or modulus operator, $\eta_{\tau,com}$ is a random variable following a uniform distribution between 0 and 1, and $\lfloor \cdot \rfloor$ is the rounding function.

If $P_{com} < L_{com}$, no pair of propagation paths will have the same delay index, yielding: $\tau_{p_1,com}^i \neq \tau_{p_2,com}^i$, where $p_1 = [0, 1, \dots, P_{com} - 1]$, $p_2 = [0, 1, \dots, P_{com} - 1]$, and $p_1 \neq p_2$.

The fractional Doppler index $\nu_{p,com}^i$ is:

$$\nu_{p,com}^i = \begin{cases} \nu_{com,max}^i, & \text{if } p_{com} = 0 \\ \lfloor 2\nu_{com,max}^i (\eta_{\nu,com} - 0.5) \rfloor, & \text{if } p_{com} > 0, \end{cases} \quad (26)$$

where $\eta_{\nu,com}$ is a random variable following a uniform distribution between 0 and 1, and $\nu_{com,max}^i$ is the maximum integer Doppler index:

$$\nu_{com,max}^i = \lceil \frac{f_c N V_{com}}{\Delta f c_0} \rceil, \quad (27)$$

with V_{com} representing the velocity of the communication receiver, f_c is the carrier frequency, c_0 is the speed of light, and $\lceil \cdot \rceil$ is the ceiling function.

C. Sensing Channel Parameters

The delay and Doppler indices for sensing, $\tau_{p,sen}^i$ and $\nu_{p,sen}^i$ respectively, are:

$$\tau_{p,sen}^i = \frac{2\Delta f M R_{p,sen}}{c_0}, \quad (28)$$

$$\nu_{p,sen}^i = \frac{2f_c N V_{p,sen}}{\Delta f c_0}, \quad (29)$$

where $R_{p,sen}$ is the range of the p_{sen}^{th} path, $V_{p,sen}$ is the velocity of the p_{sen}^{th} path, $p_{sen} = [0, 1, \dots, P_{sen} - 1]$, and P_{sen} is the number of sensing propagation paths.

As monostatic sensing is assumed, the transmitted signal is reflected from the target to the sensing receiver attached or adjacent to the transmitter, hence a factor of 2 is present in (28) and (29). The first P_t propagation paths are LoS paths associated with each sensing target, and the remaining P_n paths are NLoS paths. The total number of sensing propagation paths P_{sen} is:

$$P_{sen} = P_t + P_n. \quad (30)$$

The fading gain $\tilde{h}_{p_t,sen}$ of the p_t^{th} target is:

$$\tilde{h}_{p_t,sen} = \sqrt{\frac{\kappa_{sen}}{\kappa_{sen} + 1}} \sqrt{\alpha_{p_t}}, \quad (31)$$

where κ_{sen} is the sensing Rician K factor, and α_{p_t} is the power gain associated with the p_t^{th} LoS path, defined as:

$$\alpha_{p_t} = \frac{c_0^2 \sigma_{p_t}}{(4\pi)^3 f_c^2 R_{p,sen}^4}, \quad (32)$$

where σ_{p_t} is the radar cross-section of the p_t^{th} target.

The fading gain $\tilde{h}_{p_n,sen}$ of the p_n^{th} NLoS path is:

$$\tilde{h}_{p_n,sen} = \sqrt{\frac{1}{P_n(\kappa_{sen} + 1)}} \zeta_{p_n,sen} \min_{\forall p_t} (\sqrt{\alpha_{p_t}}), \quad (33)$$

where $\zeta_{p_n,sen}$ is a complex Gaussian random variable with mean $\mu_{sen} = 0$ and variance $\sigma_{sen}^2 = 1$, expressed as $\mathcal{N}(\mu_{sen}, \sigma_{sen}^2)$.

The NLoS power is set relative to the smallest value of α_{p_t} , which is associated with the weakest target signal. The smallest value of α_{p_t} is used to ensure that no NLoS paths have an average power higher than $\sqrt{\frac{1}{P_n(\kappa_{sen} + 1)}}$ relative to any of the targets. As the system is operating in the mmWave band, the NLoS reflections are assumed, on average, to be weaker than the LoS signals.

The range and velocity of the NLoS paths, $R_{p_n,sen}$ and $V_{p_n,sen}$, are:

$$R_{p_n,sen} = R_{n,max} \eta_{\tau,sen}, \quad (34)$$

$$V_{p_n,sen} = 2V_{n,max} (\eta_{\nu,sen} - 0.5), \quad (35)$$

where $\eta_{\tau,sen}$ and $\eta_{\nu,sen}$ are random variables following a uniform distribution between 0 and 1, and:

$$R_{n,max} = \sqrt[4]{\kappa_{sen}} \max_{\forall p_t} (R_{p_t,sen}), \quad (36)$$

$$V_{n,max} = \frac{\Delta f c_0}{4f_c}, \quad (37)$$

The fourth root of κ_{sen} is present in (36) as the power gain is inversely proportional to R^4 , as seen in (32). A maximum range is fixed, because the reflected signals having NLoS paths associated with delays larger than the maximum in (36) are assumed to not significantly interfere, due to the high attenuation associated with a greater range.

IV. Received Signal Processing

A. Communication Data Detection

The DD received signal $\tilde{\mathbf{y}} \in \mathbb{C}^{MN \times 1}$ can be represented as:

$$\tilde{\mathbf{y}} = \tilde{\mathbf{H}} \tilde{\mathbf{x}} + \tilde{\mathbf{z}}, \quad (38)$$

where $\tilde{\mathbf{z}}$ is the complex-valued AWGN in the DD.

MMSE demodulation is applied at the receiver, with perfect channel estimation assumed. The vector of estimated symbols $\hat{\mathbf{s}} \in \mathbb{C}^{N_s \times 1}$ is formulated as:

$$\hat{\mathbf{s}} = \tilde{\mathbf{G}}^H \tilde{\mathbf{y}}, \quad (39)$$

where $\tilde{\mathbf{G}}$ is:

$$\tilde{\mathbf{G}} = \left(\tilde{\mathbf{H}} \mathbf{C} \mathbf{C}^H \tilde{\mathbf{H}}^H + N_0 \mathbf{I}_{MN \times MN} \right)^{-1} \tilde{\mathbf{H}} \mathbf{C}, \quad (40)$$

where N_0 is the AWGN power, and $\mathbf{I}_{MN \times MN}$ is the $MN \times MN$ identity matrix. The estimated symbols are then demodulated to obtain the estimated bits.

B. Sensing Target Parameter Estimation

For sensing, it is assumed that the number and directions of the targets are known. A two step sensing method is applied. The first step utilises a data cancellation-based method to estimate the integer indices of the targets. The accuracy of this step is limited by the system parameters. The second step employs ML detection to estimate the fractional component of the indices estimated in step 1. The resolution of the fractional index estimation is a separate system parameter N_{ML} .

The first step is a modified data cancellation method adapted from [8]. The DD received signal can be represented as in (38), or as:

$$\tilde{\mathbf{y}} = \tilde{\mathbf{X}}_X \tilde{\mathbf{h}} + \tilde{\mathbf{z}}, \quad (41)$$

where $\tilde{\mathbf{h}} \in \mathbb{C}^{MN \times 1}$ is the vector containing the propagation path gains at the associated delay-Doppler indices, and $\tilde{\mathbf{X}}_X \in \mathbb{C}^{MN \times MN}$ is an expanded matrix of the DD transmitted signal matrix $\tilde{\mathbf{X}}$ shown in (42), where τ_1^i and $\tau_2^i = [0, 1, \dots, M-1]$, ν_1^i and $\nu_2^i = [0, 1, \dots, N-1]$, and:

$$\nu_{diff}^i = \begin{cases} \nu_1^i - \nu_2^i + N, & \text{if } \nu_1^i - \nu_2^i < 0 \\ \nu_1^i - \nu_2^i, & \text{if } \nu_1^i - \nu_2^i > 0. \end{cases} \quad (43)$$

The estimated channel parameter vector $\hat{\mathbf{h}}$ is calculated as follows:

$$\hat{\mathbf{h}} = \tilde{\mathbf{X}}_X^H \tilde{\mathbf{y}}. \quad (44)$$

The indices at which the P_t peak amplitudes of $\|\hat{\mathbf{h}}\|^2$ occur are the estimated integer delay and Doppler indices $\hat{\tau}_{pt}^{dc}$ and $\hat{\nu}_{pt}^{dc}$ of the first step, where $\|\cdot\|$ is the Euclidean norm.

The ML second step used for fractional index estimation applies ML estimation to the indices adjacent to the P_t delay and Doppler integer indices gleaned from the first step. The delay indices τ_{pt}^{ml} and Doppler indices ν_{pt}^{ml} considered for the p_t^{th} target are:

$$\tau_{pt}^{ml} = \hat{\tau}_{pt}^{dc} \mathbf{1}_{(2N_{ML}+1) \times 1} + \frac{\mathbf{n}_\tau}{N_{ML}}, \quad (45)$$

$$\nu_{pt}^{ml} = \hat{\nu}_{pt}^{dc} \mathbf{1}_{(2N_{ML}+1) \times 1} + \frac{\mathbf{n}_\nu}{N_{ML}}, \quad (46)$$

where $\mathbf{1}_{(2N_{ML}+1) \times 1}$ is a $[(2N_{ML}+1) \times 1]$ vector of 1, $\mathbf{n}_\tau = [-N_{ML}, -N_{ML}+1, \dots, 0, \dots, N_{ML}-1, N_{ML}]$, $\mathbf{n}_\nu = [-N_{ML}, -N_{ML}+1, \dots, 0, \dots, N_{ML}-1, N_{ML}]$, and N_{ML} is the interpolation or resolution refinement factor.

The ML algorithm creates a set of equivalent channels $\hat{\mathbf{H}}_{\tau_{pt}^{ml}, \nu_{pt}^{ml}}$, with a gain of 1, for the sets τ_{pt}^{ml} and ν_{pt}^{ml} . The gain is set to 1 since no channel gain estimation is performed. The algorithm calculates the peak associated with each combination, and determines the indices $\hat{\tau}_{pt}^{ml}$ and $\hat{\nu}_{pt}^{ml}$

estimated by selecting the combination with the largest peak, following [38]:

$$(\hat{\tau}_{pt}^{ml}, \hat{\nu}_{pt}^{ml}) = \arg \max_{\forall \tau_{pt}^{ml}, \nu_{pt}^{ml}} \frac{\|\tilde{\mathbf{x}}^H \hat{\mathbf{H}}_{\tau_{pt}^{ml}, \nu_{pt}^{ml}}^H \tilde{\mathbf{y}}\|^2}{\tilde{\mathbf{x}}^H \hat{\mathbf{H}}_{\tau_{pt}^{ml}, \nu_{pt}^{ml}}^H \hat{\mathbf{H}}_{\tau_{pt}^{ml}, \nu_{pt}^{ml}} \tilde{\mathbf{x}}}, \quad (47)$$

where $\tilde{\mathbf{y}}$ is the DD received signal vector.

The indices $\hat{\tau}_{pt}^{ml}$ and $\hat{\nu}_{pt}^{ml}$ are then used to calculate the target range $\hat{R}_{pt, sen}$ and velocity $\hat{V}_{pt, sen}$, following [36]:

$$\hat{R}_{pt, sen} = \frac{\hat{\tau}_{pt}^{ml} c_0}{2Mf_s}, \quad (48)$$

$$\hat{V}_{pt, sen} = \frac{\hat{\nu}_{pt}^{ml} \Delta f c_0}{2Nf_c}. \quad (49)$$

V. Cramér-Rao Bound

Following [39], the average unbiased estimator CRBs for the associated range and velocity estimation are defined as:

$$\hat{\sigma}_{l, R}^2 \geq \frac{N_0}{P_{avg} |\tilde{h}_{pt, sen}|^2 \pi^2 MN (M-1)^2} \left(\frac{c_0}{2\Delta f} \right)^2, \quad (50)$$

$$\hat{\sigma}_{l, V}^2 \geq \frac{N_0}{P_{avg} |\tilde{h}_{pt, sen}|^2 \pi^2 MN (N-1)^2} \left(\frac{c_0 \Delta f}{2f_c} \right)^2, \quad (51)$$

where $\hat{\sigma}_{l, R}^2$ and $\hat{\sigma}_{l, V}^2$ are the variance of the target range and of the velocity estimation errors, respectively, while P_{avg} is the average power of the transmitted signal.

As the RMSE is the metric used for sensing, the standard deviation is utilised:

$$\hat{\sigma}_{l, R} \geq \sqrt{\frac{N_0}{P_{avg} |\tilde{h}_{pt, sen}|^2 \pi^2 MN (M-1)^2} \frac{c_0}{2\Delta f}}, \quad (52)$$

$$\hat{\sigma}_{l, V} \geq \sqrt{\frac{N_0}{P_{avg} |\tilde{h}_{pt, sen}|^2 \pi^2 MN (N-1)^2} \frac{c_0 \Delta f}{2f_c}}, \quad (53)$$

where $\hat{\sigma}_{l, R}$ and $\hat{\sigma}_{l, V}$ are the standard deviations of the target range and velocity estimation errors, respectively.

It is important to note that this CRB is an average CRB, not a true lower bound.

VI. Computational Complexity Analysis

This section quantifies the additional complexity introduced by CDMA/OTFS to the modulation and communication demodulation compared to OTFS, and the complexity of the target parameter estimation methods.

A. Additional Modulation and Demodulation Complexity Compared to OTFS

In (3), the modulation relies on a multiplication of an $(MN \times N_s)$ matrix by an $(N_s \times 1)$ vector. The computational

$$\tilde{\mathbf{X}}_X[\tau_1^i + M\nu_1^i, \tau_2^i + M\nu_2^i] = \begin{cases} \tilde{\mathbf{X}}[\tau_1^i - \tau_2^i + M, \nu_{diff}^i] e^{\frac{j2\pi\nu_2^i(\tau_1^i - \tau_2^i)}{MN}}, & \text{if } \tau_1^i - \tau_2^i < 0 \\ \tilde{\mathbf{X}}[\tau_1^i - \tau_2^i, \nu_{diff}^i] e^{\frac{j2\pi\nu_2^i(\tau_1^i - \tau_2^i)}{MN}}, & \text{if } \tau_1^i - \tau_2^i > 0, \end{cases} \quad (42)$$

complexity of this operation is on the order of $O(MNN_s)$, for all the CDMA/OTFS schemes.

For DI-CDMA/OTFS, $N_s = N_{mult}N$, $1 \leq N_{mult} \leq M$, hence the complexity at the minimum and maximum throughputs is $O(MN^2)$ and $O(M^2N^2)$, respectively.

For Dp-CDMA/OTFS, $N_s = N_{mult}M$, $1 \leq N_{mult} \leq N$, hence the complexity at the minimum and maximum throughputs is $O(M^2N)$ and $O(M^2N^2)$, respectively.

For DD-CDMA/OTFS, $N_s = N_{mult}$, $1 \leq N_{mult} \leq MN$, hence the complexity at the minimum and maximum throughputs is $O(MN)$ and $O(M^2N^2)$, respectively.

The computational complexity of all the CDMA/OTFS schemes is the same for the same throughput. Modulating using (4) for DI-CDMA/OTFS and (9) for Dp-CDMA/OTFS leads to the same complexity.

For MMSE demodulation, there is an additional matrix multiplication required in (40), where the channel matrix ($MN \times MN$) is multiplied by the spreading matrix ($MN \times N_s$). This multiplication can be performed once, with the resulting matrix used three times in (40). The complexity of the multiplication is on the order of $O(M^2N^2N_s)$.

B. Complexity of the Sensing Methods

There are $MN \times MN$ operations required for the creation of the expanded matrix of the DD transmitted signal (42), hence the complexity is $O(M^2N^2)$. The complexity of the matrix multiplication of the data cancellation method (44) is $O(MN \times MN \times 1) = O(M^2N^2)$, since an ($MN \times MN$) matrix is multiplied by an ($MN \times 1$) vector. The total complexity of this algorithm is therefore $O(2M^2N^2)$.

The computational complexity of (47) for fractional index estimation is $O(2MN)$. This operation is repeated $(2N_{ML} + 1)^2$ times, hence the total complexity of the ML fractional index estimation is $O(2MN(2N_{ML} + 1)^2)$.

C. Discussions

The additional complexity imposed on the modulation by CDMA/OTFS is comparable to that of SCMA OTFS schemes, as both involve the spreading of symbols across the available resources. There exist certain matrix multiplication methods having reduced complexity for sparse matrices, so the additional complexity of SCMA OTFS may be reduced, depending on the spreading matrix structure. Other multi-user methods, such as directly allocating DD indices to users [25]–[27], may have a lower modulation complexity, depending on their modulation structure.

The additional demodulation complexity of CDMA/OTFS is much lower than that of DD index allocation, because the properties of the dense sequences chosen for CDMA/OTFS allow for a relatively simple demodulation, due to their desirable cross-correlation properties. Although no correlation operations are harnessed for communication detection and demodulation, the low cross-correlation of the sequences mitigates inter-user/inter-symbol interference. This trend becomes more pronounced when perfectly orthogonal sequences

TABLE 3: Communication simulation parameters

Variable	Value
Carrier frequency f_c	40 GHz
Subcarrier spacing Δf	120 kHz
Number of communication delay taps L_{com}	3
Number of communication propagation paths P_{com}	3
Rician K factor κ_{com}	0 dB
Number of subcarriers M	64
Number of symbols sent per frame N	64
Communication receiver velocity	200 m/s
Minimum number of bit errors	600
Maximum number of bits simulated	1×10^7

having zero-cross-correlation are employed. DD index allocation requires more complex demodulation methods, for example, iterative methods such as successive interference cancellation, in order to mitigate the inter-symbol and inter-user interference.

VII. Simulation Results and Discussions

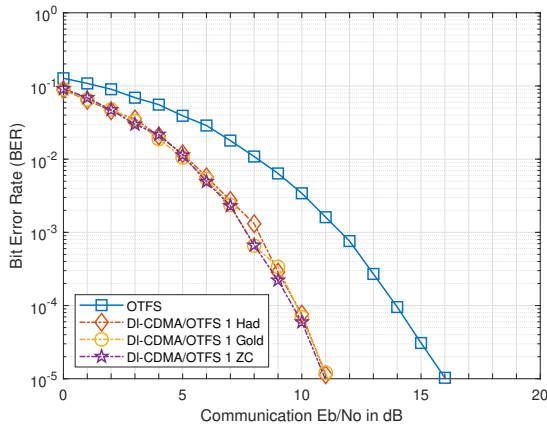
This section discusses the BER results and sensing RMSE results of both multi-user CDMA/OTFS and single-user OTFS. The single-user OTFS system assigns a single symbol to each DD resource, hence transmitting MN symbols in a frame. In the legend, “Gold” refers to Gold sequence spreading, “Had” refers to Hadamard sequence spreading, and “ZC” refers to Zadoff-Chu sequence spreading.

A. Communication BER Results

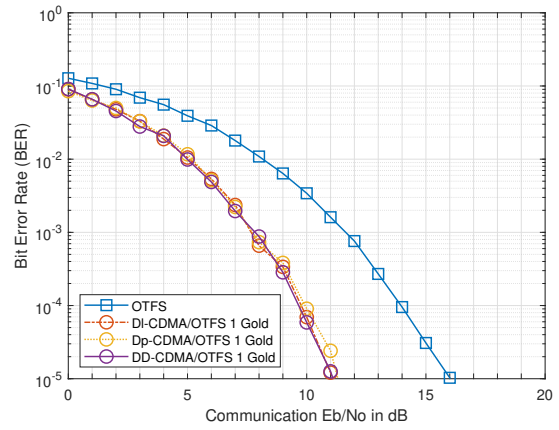
The simulation parameters used are shown in Table 3. The BER of Quadrature Phase Shift Keying (QPSK) Gold, Hadamard, and Zadoff-Chu sequence spreading for DI-CDMA/OTFS, Dp-CDMA/OTFS, and DD-CDMA/OTFS is portrayed in Figure 1 for $N_{mult} = 1$. The BER of OTFS QPSK is also shown in Figure 1. At the minimum throughput, all system configurations relying on the three sequences have similar BER performances. The BER of CDMA/OTFS for $N_{mult} = 1$ is much lower than that of OTFS, albeit at a large cost of throughput, which is reduced by a factor of 64 for DI-CDMA/OTFS and Dp-CDMA/OTFS, and a factor of 4096 for DD-CDMA/OTFS.

The performance of Hadamard sequences for $N_{mult} = 1$ depends on the specific Hadamard sequence selected, as shown in Figure 2. When the first Hadamard sequence of the Hadamard matrix is selected (Hadamard sequence 1), the BER for CDMA/OTFS is higher than that of OTFS, as this sequence is a vector of 1.

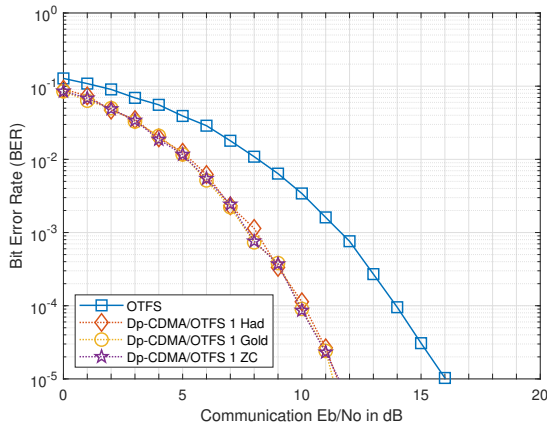
The BER of QPSK Gold, Hadamard, and Zadoff-Chu sequence spreading for $N_{mult} = 32$ for DI-CDMA/OTFS and Dp-CDMA/OTFS, $N_{mult} = 2048$ for DD-CDMA/OTFS, and of OTFS QPSK is shown in Figure 3 for a throughput of 1 bpcu for CDMA/OTFS. For 1 bpcu, the Zadoff-Chu sequence outperforms OTFS for all spreading configurations,



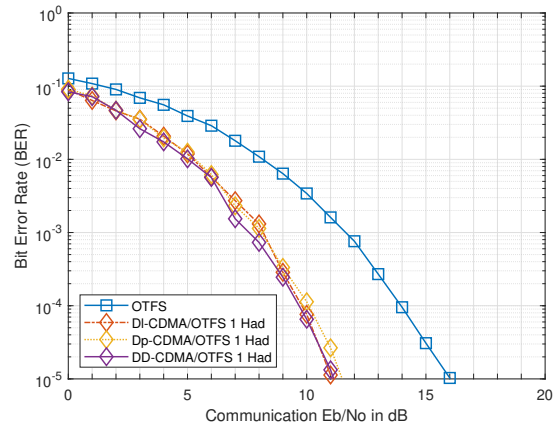
(a) OTFS and DI-CDMA/OTFS



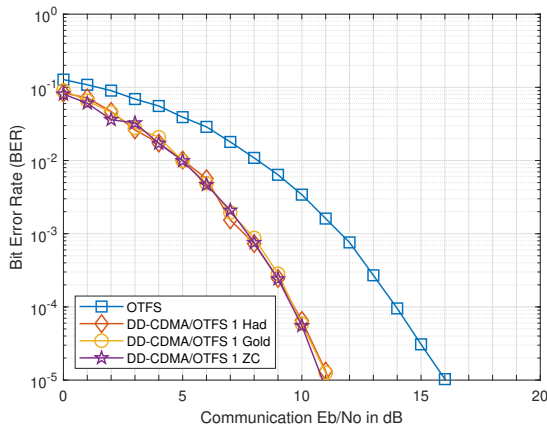
(b) OTFS and Gold sequence



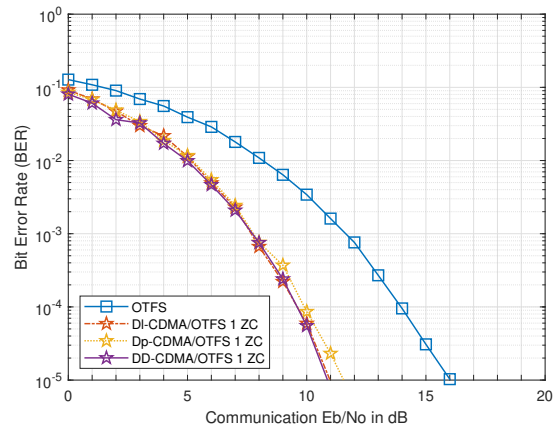
(c) OTFS and Dp-CDMA/OTFS



(d) OTFS and Hadamard sequence



(e) OTFS and DD-CDMA/OTFS



(f) OTFS and Zadoff-Chu sequence

FIGURE 1: BER of QPSK Gold, Hadamard, and Zadoff-Chu sequence spreading for $N_{mult} = 1$ for DI-CDMA/OTFS, Dp-CDMA/OTFS, and DD-CDMA/OTFS, and of OTFS QPSK

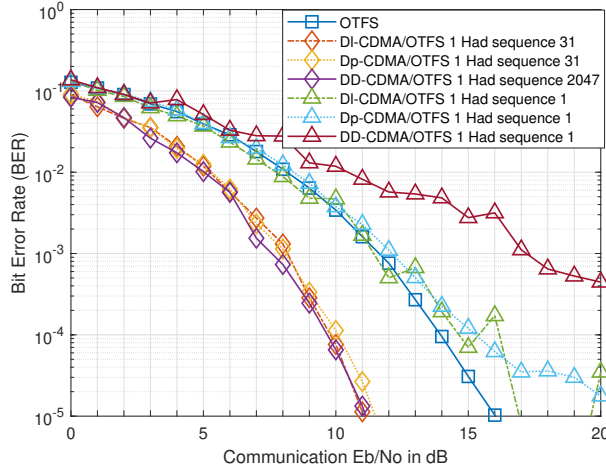


FIGURE 2: BER of QPSK Hadamard sequences 1 and 31 spreading for $N_{mult} = 1$ for DI-CDMA/OTFS and Dp-CDMA/OTFS, Hadamard sequences 1 and 2047 spreading for DD-CDMA/OTFS, and of OTFS QPSK

as Zadoff-Chu sequences are resistant to delay and Doppler interference. The BER of Gold sequence spreading is similar to that of OTFS for all spreading configurations, with the BER of Gold DD-CDMA/OTFS slightly lower than that of OTFS at high Energy per bit over Noise power (E_b/N_0). This is because the length of the Gold sequences for DD-CDMA/OTFS is longer than for DI-CDMA/OTFS and Dp-CDMA/OTFS. The BER performance of Hadamard DI-CDMA/OTFS and Dp-CDMA/OTFS is similar to OTFS for the majority of the E_b/N_0 range, but its BER is slightly higher at larger E_b/N_0 , as Hadamard sequences are vulnerable to multi-path interference. The BER of Hadamard DD-CDMA/OTFS is higher than that of OTFS, since the spreading sequence experiences multi-path interference in both the delay and Doppler domains.

The BER of QPSK Gold, Hadamard, and Zadoff-Chu sequence spreading for $N_{mult} = 64$ for DI-CDMA/OTFS and Dp-CDMA/OTFS, $N_{mult} = 4096$ for DD-CDMA/OTFS, and of OTFS QPSK is shown in Figure 4, for a throughput of 2 bpcu. At 2 bpcu, the performance of Gold sequences is poor, as their lack of orthogonality leads to increased inter-symbol interference. The BER of Zadoff-Chu sequences is almost identical to OTFS. The BER for 2 bpcu is higher than for a throughput of 1 bpcu, as the sequences experience a small amount of inter-symbol interference, despite their orthogonality. The performance of Hadamard sequences is similar to the half throughput case of 1 bpcu, as the sequences experience little inter-symbol interference due to their orthogonality to each other.

B. Sensing RMSE Results

The simulation parameters used are shown in Table 4. The range and velocity RMSE of QPSK OTFS are shown in Figure 5 for $N_{ML} = 1, 4, \text{ and } 8$, $R_t = 500$ m, $V_t = 200$

TABLE 4: Sensing simulation parameters

Variable	Value
Carrier frequency f_c	40 GHz
Subcarrier spacing Δf	120 kHz
Number of sensing targets P_t	1
Rician K factor κ_{sen}	10 dB
Number of subcarriers M	64
Number of symbols sent per frame N	64
Number of frames simulated per E_b/N_0	4000

m/s, and $P_n = 0$ NLoS paths. The RMSE is dominated by the integer index estimation at E_b/N_0 below -18 dB, but by the fractional index estimation at higher E_b/N_0 . As N_{ML} is increased, the system resolution is increased, which leads to a potentially lower error floor, as seen in Figure 5a.

In Figure 5b, the closest fractional index to the target velocity is unchanged for $N_{ML} = 4$ and 8, hence the error floor is identical. As N_{ML} is increased, the fractional index detection algorithm becomes more sensitive to AWGN, which leads to the RMSE of the estimate reaching the error floor at higher E_b/N_0 than for $N_{ML} = 4$. All subsequent results use $N_{ML} = 8$.

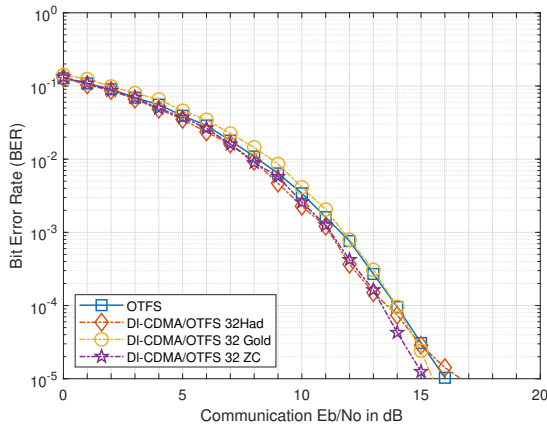
In Figure 5b, the error floor is higher than the CRB, but in Figure 5a, the error floor is lower than the CRB for $N_{ML} = 8$. This is due to the discrete properties of the estimator. The target parameter estimator outputs a value from a discrete set, whereas the CRB assumes a continuous set. Hence, when the discrete estimator output is close to the target parameter value, the sensing error can be smaller than the CRB in the E_b/N_0 range considered. At higher E_b/N_0 , the CRB will reduce further, below the error floor.

As similar trends are observed for range and velocity estimation, only the range RMSE results will be presented.

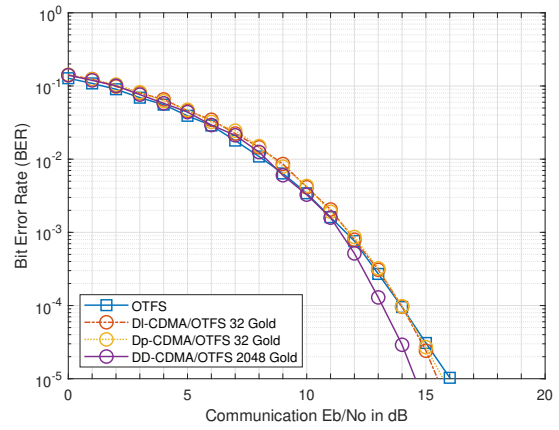
The range RMSE of QPSK Gold, Hadamard, and Zadoff-Chu sequence spreading are shown in Figure 6 for $N_{mult} = 64$ for DI-CDMA/OTFS and Dp-CDMA/OTFS, $N_{mult} = 4096$ for DD-CDMA/OTFS, and of OTFS QPSK for $N_{ML} = 8$, $R_t = 500$ m, $V_t = 200$ m/s, and $P_n = 0$ NLoS paths.

For most of the CDMA/OTFS systems, the E_b/N_0 at which the RMSE is dominated by the fractional index estimation error is 1 dB lower than for OTFS, except for Hadamard DI-CDMA/OTFS, Gold and Zadoff-Chu Dp-CDMA/OTFS, where it is 2dB lower than for OTFS. This is because the spreading codes distribute the signal over multiple indices, thereby creating a more uniform transmitted signal compared to OTFS. It has been shown [35] that more deterministic signals lead to a superior sensing performance.

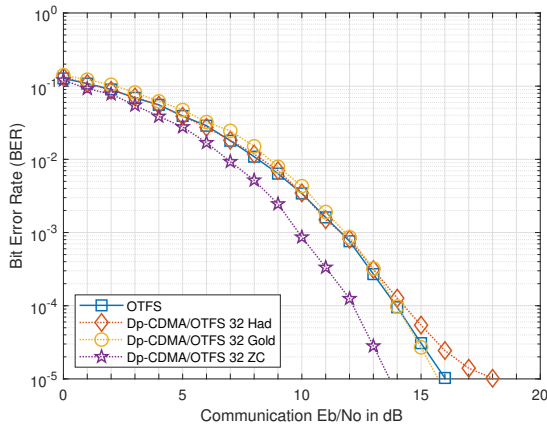
The range RMSE of QPSK Gold, Hadamard, and Zadoff-Chu sequence spreading are shown in Figure 7 for $N_{mult} = 64$ for DI-CDMA/OTFS and Dp-CDMA/OTFS, $N_{mult} = 4096$ for DD-CDMA/OTFS, and of OTFS QPSK for $N_{ML} = 8$, $R_t = 200$ m, $V_t = 110$ m/s, and $P_n = 7$ NLoS paths.



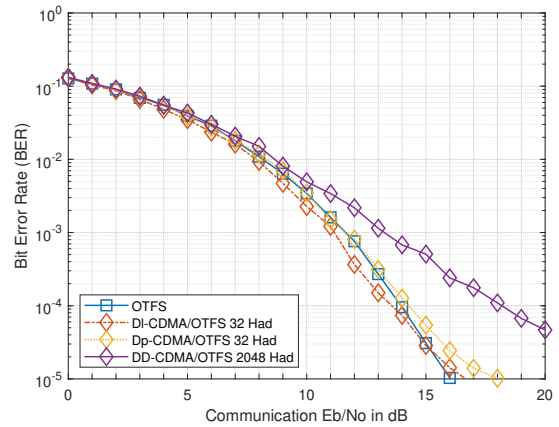
(a) OTFS and DI-CDMA/OTFS



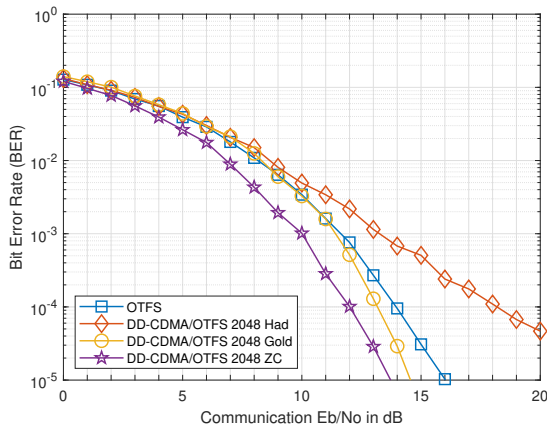
(b) OTFS and Gold sequence



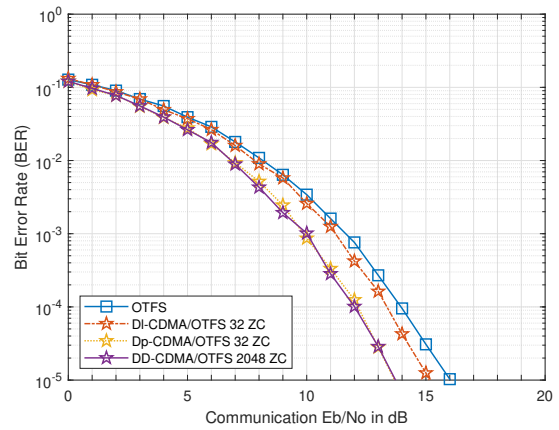
(c) OTFS and Dp-CDMA/OTFS



(d) OTFS and Hadamard sequence

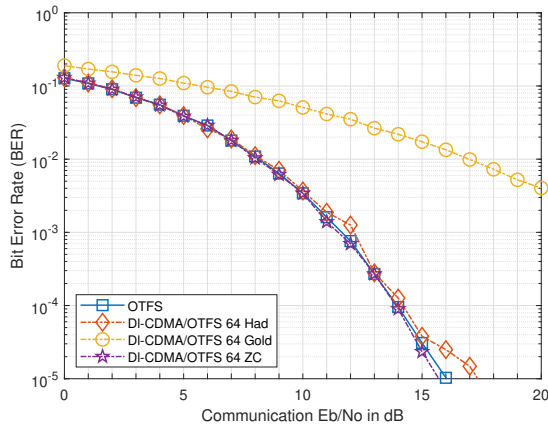


(e) OTFS and DD-CDMA/OTFS

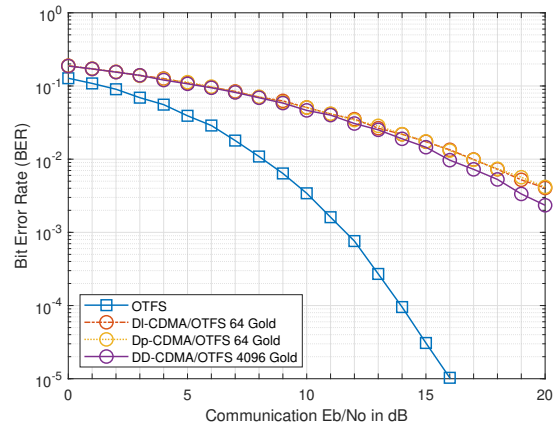


(f) OTFS and Zadoff-Chu sequence

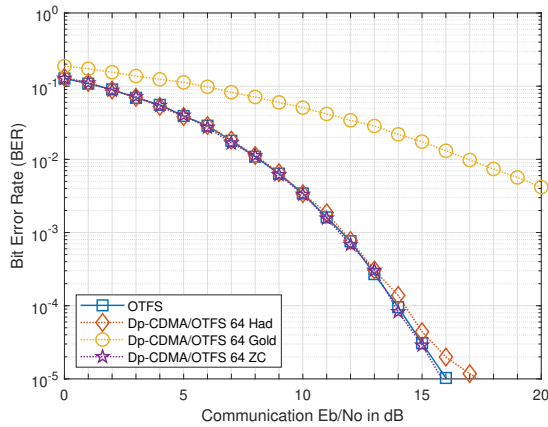
FIGURE 3: BER of QPSK Gold, Hadamard, and Zadoff-Chu sequence spreading for $N_{mult} = 32$ for DI-CDMA/OTFS and Dp-CDMA/OTFS, $N_{mult} = 2048$ for DD-CDMA/OTFS, and of OTFS QPSK



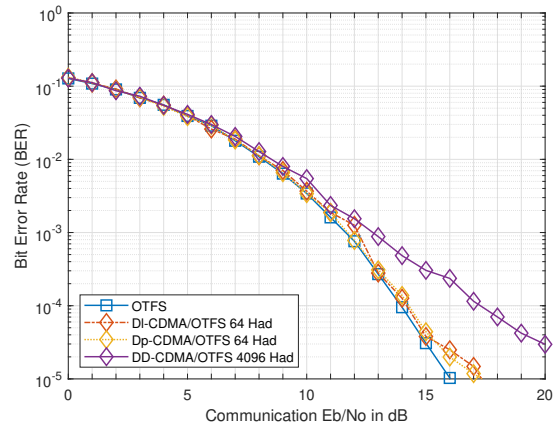
(a) OTFS and DI-CDMA/OTFS



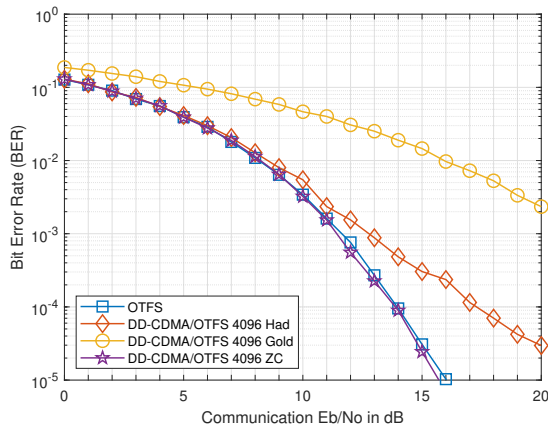
(b) OTFS and Gold sequence



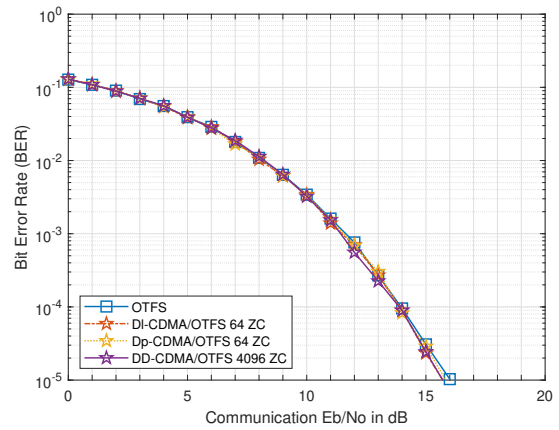
(c) OTFS and Dp-CDMA/OTFS



(d) OTFS and Hadamard sequence



(e) OTFS and DD-CDMA/OTFS



(f) OTFS and Zadoff-Chu sequence

FIGURE 4: BER of QPSK Gold, Hadamard, and Zadoff-Chu sequence spreading for $N_{mult} = 64$ for DI-CDMA/OTFS and Dp-CDMA/OTFS, $N_{mult} = 4096$ for DD-CDMA/OTFS, and of OTFS QPSK

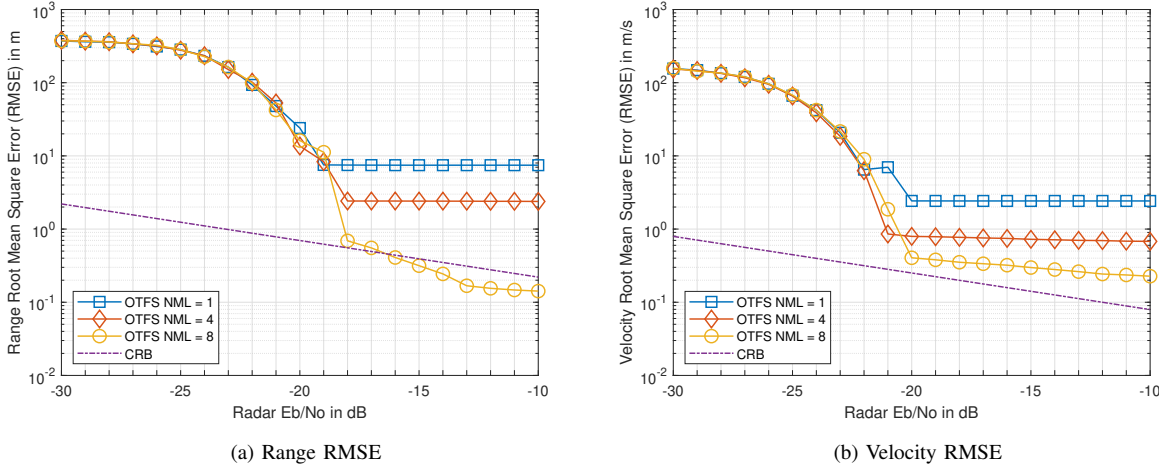


FIGURE 5: Range and velocity RMSE of OTFS QPSK for $N_{ML} = 1, 4,$ and $8, R_t = 500$ m, $V_t = 200$ m/s, and $P_n = 0$ NLoS paths

TABLE 5: Eb/No at which a BER of 10^{-4} is reached for CDMA/OTFS at half load relative to OTFS

Configuration \ Sequence	Gold	Hadamard	Zadoff-Chu
DI-CDMA/OTFS	0 dB	0 dB	-0.5 dB
Dp-CDMA/OTFS	0 dB	0 dB	-2 dB
DD-CDMA/OTFS	-1 dB	+4 dB	-2 dB

TABLE 6: Eb/No at which a BER of 10^{-4} is reached for CDMA/OTFS at full load relative to OTFS

Configuration \ Sequence	Gold	Hadamard	Zadoff-Chu
DI-CDMA/OTFS	N/A	0 dB	0 dB
Dp-CDMA/OTFS	N/A	0 dB	0 dB
DD-CDMA/OTFS	N/A	+3 dB	0 dB

For most of the CDMA/OTFS systems, the Eb/No at which the RMSE is dominated by the fractional index estimation error is 1 dB lower than for OTFS, except for Zadoff-Chu Dp-CDMA/OTFS and Gold DD-CDMA/OTFS, where it is at the same Eb/No as OTFS. As the velocity is decreased, the sensing performance advantage of CDMA/OTFS is slightly decreased, as the distortion caused by the Doppler shifts of the propagation paths is reduced.

VIII. Conclusions

Three different configurations of CDMA/OTFS were introduced. The multi-user communication performance of Zadoff-Chu CDMA/OTFS is similar to that of single user OTFS at an equal throughput. When fewer users are present, the multi-user throughput is diminished, and Zadoff-Chu CDMA/OTFS has a lower BER than single user OTFS.

TABLE 7: Eb/No at which the RMSE is dominated by fractional index estimation error relative to OTFS at full load, for a target velocity of 200 m/s

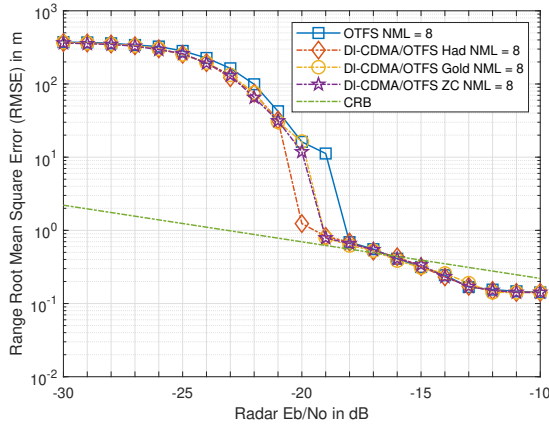
Configuration \ Sequence	Gold	Hadamard	Zadoff-Chu
DI-CDMA/OTFS	-1 dB	-2 dB	-1 dB
Dp-CDMA/OTFS	-2 dB	-1 dB	-2 dB
DD-CDMA/OTFS	-1 dB	-1 dB	-1 dB

TABLE 8: Eb/No at which the RMSE is dominated by fractional index estimation error relative to OTFS at full load, for a target velocity of 110 m/s

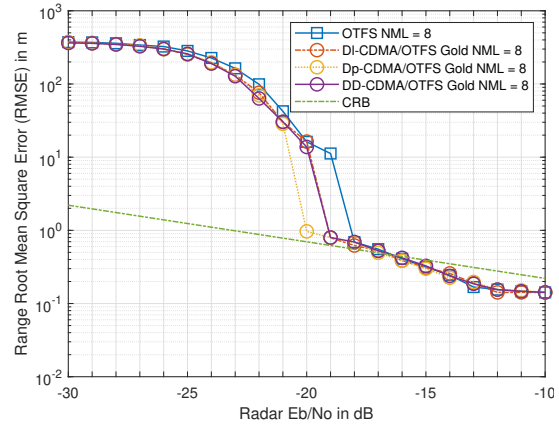
Configuration \ Sequence	Gold	Hadamard	Zadoff-Chu
DI-CDMA/OTFS	-1 dB	-1 dB	-1 dB
Dp-CDMA/OTFS	-1 dB	-1 dB	0 dB
DD-CDMA/OTFS	0 dB	-1 dB	-1 dB

The communication performance of Zadoff-Chu sequences is similar for all three CDMA/OTFS spreading configurations. Gold and Hadamard sequences do not consistently outperform single user OTFS communication. The communication performance of the different configurations relative to OTFS at the normalised half and full load are summarised in Tables 5 and 6, respectively.

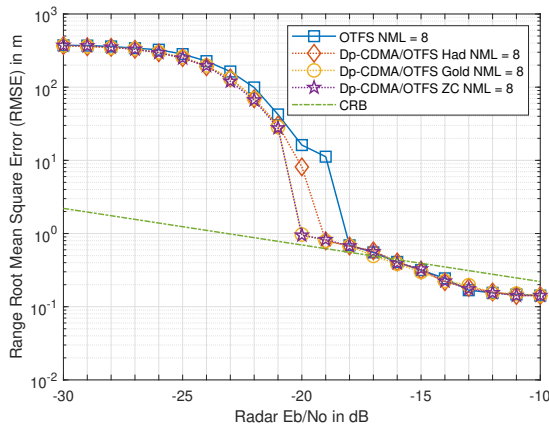
The three CDMA/OTFS spreading configurations outperform pure OTFS sensing for all the velocities considered. Hadamard sequences lead to a superior sensing performance for DI-CDMA/OTFS at high velocities, but the three sequences have a similar performance at lower velocities. Gold sequences increase the sensing performance of Dp-CDMA/OTFS at high velocities, whereas Zadoff-Chu se-



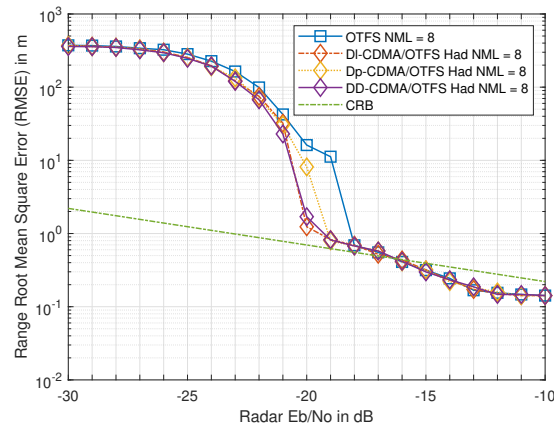
(a) OTFS and DI-CDMA/OTFS



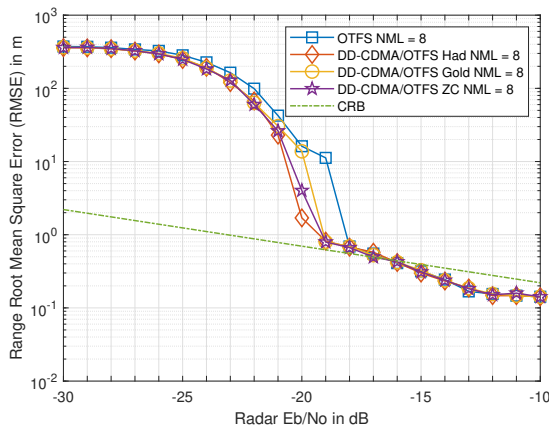
(b) OTFS and Gold sequence



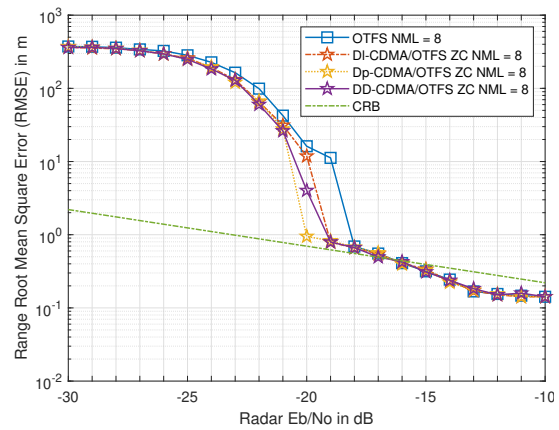
(c) OTFS and Dp-CDMA/OTFS



(d) OTFS and Hadamard sequence

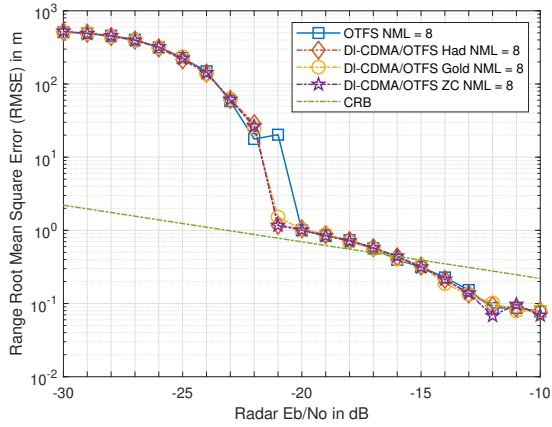


(e) OTFS and DD-CDMA/OTFS

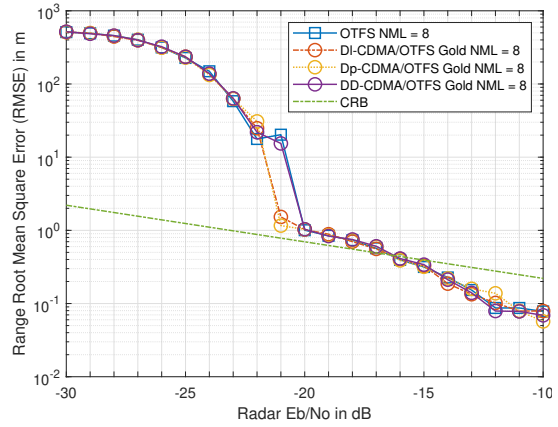


(f) OTFS and Zadoff-Chu sequence

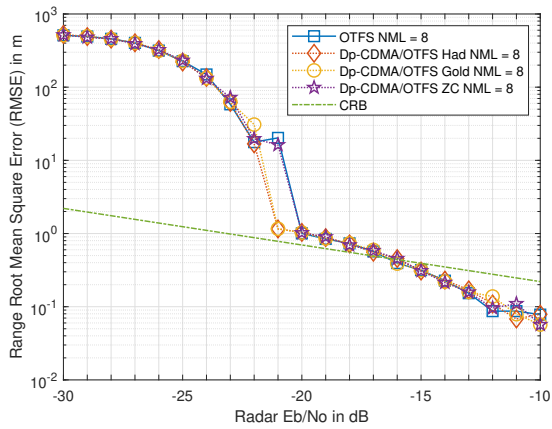
FIGURE 6: Range RMSE of QPSK Gold, Hadamard, and Zadoff-Chu sequence spreading for $N_{mult} = 64$ for DI-CDMA/OTFS and Dp-CDMA/OTFS, $N_{mult} = 4096$ for DD-CDMA/OTFS, and of OTFS QPSK for $N_{ML} = 8$, $R_t = 500$ m, $V_t = 200$ m/s, and $P_n = 0$ NLoS paths



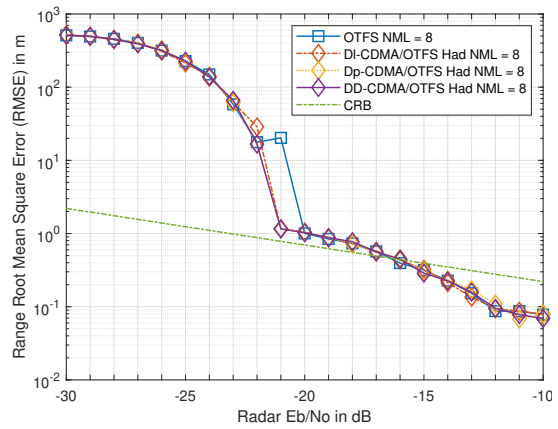
(a) OTFS and DI-CDMA/OTFS



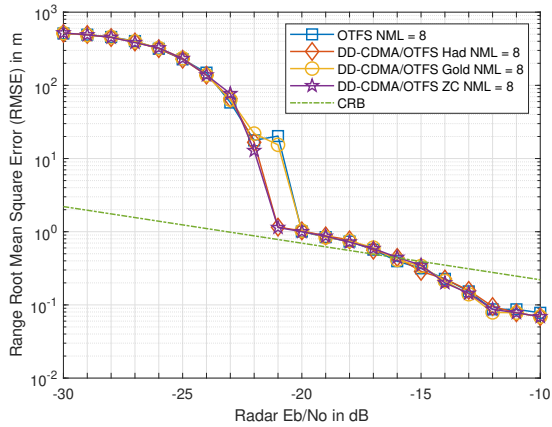
(b) OTFS and Gold sequence



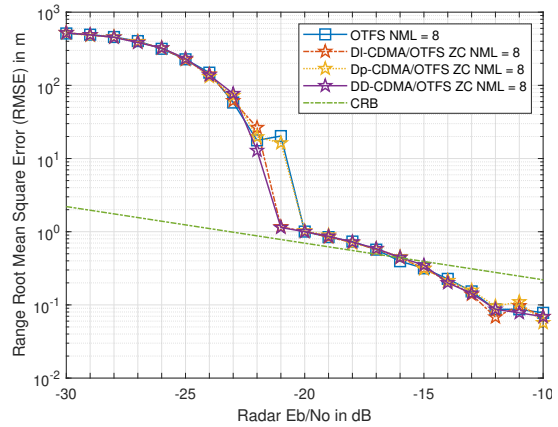
(c) OTFS and Dp-CDMA/OTFS



(d) OTFS and Hadamard sequence



(e) OTFS and DD-CDMA/OTFS



(f) OTFS and Zadoff-Chu sequence

FIGURE 7: Range RMSE of QPSK Gold, Hadamard, and Zadoff-Chu sequence spreading for $N_{mult} = 64$ for DI-CDMA/OTFS and Dp-CDMA/OTFS, $N_{mult} = 4096$ for DD-CDMA/OTFS, and of OTFS QPSK for $N_{ML} = 8$, $R_t = 200$ m, $V_t = 110$ m/s, and $P_n = 7$ NLoS paths

quences lead to the similar sensing performance as pure OTFS at lower velocities. The sensing performance of DD-CDMA/OTFS is similar for all three sequence types at high velocities, but Gold sequences lead to an inferior sensing performance at low velocities. The sensing performance of the different configurations relative to OTFS at full load are summarised in Tables 7 and 8, for target velocities of 200 m/s and 110 m/s respectively.

Following these results, Zadoff-Chu DI-CDMA/OTFS and DD-CDMA/OTFS are the configurations that consistently outperform pure OTFS sensing, whilst maintaining a similar communication performance at the same throughput.

The added modulation complexity of CDMA/OTFS is similar to other OTFS multi-user methodologies, but the demodulation complexity of CDMA/OTFS is lower than that of some other OTFS multi-user methodologies. CDMA/OTFS sensing can also consistently outperform OTFS sensing whilst not requiring any additional complexity for target parameter estimation. Hence, CDMA/OTFS is a computationally more attractive multi-user approach for OTFS ISAC than the alternatives in the literature.

Future work will consider SCMA-OTFS ISAC, as there is much interest in the employment of sparse codes for multi-user systems [29]–[31], [34], [40]–[43]. The sparsity of these codes is expected to reduce the sensing performance, hence methods of mitigating this effect have to be developed.

REFERENCES

- [1] F. Liu, C. Masouros, A. P. Petropulu, H. Griffiths, and L. Hanzo, "Joint Radar and Communication Design: Applications, State-of-the-Art, and the Road Ahead," *IEEE Transactions on Communications*, vol. 68, no. 6, pp. 3834–3862, 2020.
- [2] F. Liu, C. Masouros, A. Li, H. Sun, and L. Hanzo, "MU-MIMO Communications With MIMO Radar: From Co-Existence to Joint Transmission," *IEEE Transactions on Wireless Communications*, vol. 17, no. 4, pp. 2755–2770, 2018.
- [3] X. Li, Y. Cui, J. A. Zhang, F. Liu, D. Zhang, and L. Hanzo, "Integrated Human Activity Sensing and Communications," *IEEE Communications Magazine*, vol. 61, no. 5, pp. 90–96, 2023.
- [4] S. Lu, F. Liu, Y. Li, K. Zhang, H. Huang, J. Zou, X. Li, Y. Dong, F. Dong, J. Zhu, Y. Xiong, W. Yuan, Y. Cui, and L. Hanzo, "Integrated Sensing and Communications: Recent Advances and Ten Open Challenges," *IEEE Internet of Things Journal*, vol. 11, no. 11, pp. 19094–19120, 2024.
- [5] R. Hadani, S. Rakib, M. Tsatsanis, A. Monk, A. J. Goldsmith, A. F. Molisch, and R. Calderbank, "Orthogonal Time Frequency Space Modulation," in *2017 IEEE Wireless Communications and Networking Conference (WCNC)*, 2017, pp. 1–6.
- [6] R. Hadani and A. Monk, "OTFS: A New Generation of Modulation Addressing the Challenges of 5G," 2018. [Online]. Available: <https://arxiv.org/abs/1802.02623>
- [7] Z. Wei, W. Yuan, S. Li, J. Yuan, G. Bharatula, R. Hadani, and L. Hanzo, "Orthogonal Time-Frequency Space Modulation: A Promising Next-Generation Waveform," *IEEE Wireless Communications*, vol. 28, no. 4, pp. 136–144, 08 2021.
- [8] P. Raviteja, K. T. Phan, Y. Hong, and E. Viterbo, "Orthogonal Time Frequency Space (OTFS) Modulation Based Radar System," in *2019 IEEE Radar Conference (RadarConf)*, 2019, pp. 1–6.
- [9] L. Gaudio, M. Kobayashi, G. Caire, and G. Colavolpe, "On the Effectiveness of OTFS for Joint Radar Parameter Estimation and Communication," *IEEE Transactions on Wireless Communications*, vol. 19, no. 9, pp. 5951–5965, 2020.
- [10] K. Zhang, Z. Li, W. Yuan, Y. Cai, and F. Gao, "Radar sensing via OTFS signaling," *China Communications*, vol. 20, no. 9, pp. 34–45, 2023.
- [11] J. Zhang, L. Cai, and H. Liu, "Integrated Sensing and Communication via Orthogonal Time Frequency Space Signaling with Hybrid Message Passing Detection and Fractional Parameter Estimation," *Sensors*, vol. 23, no. 24, 2023. [Online]. Available: <https://www.mdpi.com/1424-8220/23/24/9874>
- [12] Z. Tang, Z. Jiang, W. Pan, and L. Zeng, "The Estimation Method of Sensing Parameters Based on OTFS," *IEEE Access*, vol. 11, pp. 66035–66049, 2023.
- [13] S. P. Muppaneni, S. R. Mattu, and A. Chockalingam, "Channel and Radar Parameter Estimation With Fractional Delay-Doppler Using OTFS," *IEEE Communications Letters*, vol. 27, no. 5, pp. 1392–1396, 2023.
- [14] T. Thaj, E. Viterbo, and Y. Hong, "Orthogonal Time Sequency Multiplexing Modulation: Analysis and Low-Complexity Receiver Design," *IEEE Transactions on Wireless Communications*, vol. 20, no. 12, pp. 7842–7855, 2021.
- [15] S. G. Neelam and P. R. Sahu, "Iterative Channel Estimation and Data Detection of OTSM With Superimposed Pilot Scheme and PAPR Analysis," *IEEE Communications Letters*, vol. 27, no. 8, pp. 2147–2151, 2023.
- [16] Z. Sui, S. Yan, H. Zhang, S. Sun, Y. Zeng, L.-L. Yang, and L. Hanzo, "Performance Analysis and Approximate Message Passing Detection of Orthogonal Time Sequency Multiplexing Modulation," *IEEE Transactions on Wireless Communications*, vol. 23, no. 3, pp. 1913–1928, 2024.
- [17] A. Doosti-Aref, E. Basar, and H. Arslan, "Sequency Index Modulation: A Novel Index Modulation for Delay-Sequency Domain Waveforms," *IEEE Wireless Communications Letters*, vol. 12, no. 11, pp. 1911–1915, 2023.
- [18] A. Doosti-Aref, C. Masouros, E. Basar, and H. Arslan, "Pairwise Sequency Index Modulation With OTSM for Green and Robust Single-Carrier Communications," *IEEE Wireless Communications Letters*, vol. 13, no. 4, pp. 1083–1087, 2024.
- [19] S. G. Neelam and P. R. Sahu, "Estimation and Compensation of IQ Imbalance for OTSM Systems," *IEEE Wireless Communications Letters*, vol. 11, no. 9, pp. 1885–1889, 2022.
- [20] —, "Joint Estimation and Compensation of CFO, IQ Imbalance and Channel Parameters for Zero Padded OTSM Systems," *IEEE Wireless Communications Letters*, vol. 12, no. 11, pp. 1871–1875, 2023.
- [21] —, "Joint Compensation of TX/RX IQ Imbalance and Channel Parameters for OTSM Systems," *IEEE Communications Letters*, vol. 27, no. 3, pp. 976–980, 2023.
- [22] A. Singh, S. Sharma, M. Sharma, and K. Deka, "Low Complexity Deep-Decoder for OTSM With Hardware Impairments," *IEEE Communications Letters*, vol. 27, no. 12, pp. 3240–3244, 2023.
- [23] B. V. S. Reddy, C. Velampalli, and S. S. Das, "Performance Analysis of Multi-User OTFS, OTSM, and Single Carrier in Uplink," *IEEE Transactions on Communications*, vol. 72, no. 3, pp. 1428–1443, 2024.
- [24] N. V. Kalpage, P. Priya, and Y. Hong, "DCT-Based OTFS With Reduced PAPR," *IEEE Communications Letters*, vol. 28, no. 1, pp. 158–162, 2024.
- [25] G. D. Surabhi, R. M. Augustine, and A. Chockalingam, "Multiple Access in the Delay-Doppler Domain using OTFS modulation," 2019. [Online]. Available: <https://arxiv.org/abs/1902.03415>
- [26] V. Khammammetti and S. K. Mohammed, "OTFS-Based Multiple-Access in High Doppler and Delay Spread Wireless Channels," *IEEE Wireless Communications Letters*, vol. 8, no. 2, pp. 528–531, 2019.
- [27] Y. Ge, Q. Deng, P. C. Ching, and Z. Ding, "OTFS Signaling for Uplink NOMA of Heterogeneous Mobility Users," *IEEE Transactions on Communications*, vol. 69, no. 5, pp. 3147–3161, 2021.
- [28] Y. Ma, G. Ma, N. Wang, Z. Zhong, and B. Ai, "OTFS-TSMA for Massive Internet of Things in High-Speed Railway," *IEEE Transactions on Wireless Communications*, vol. 21, no. 1, pp. 519–531, 2022.
- [29] A. Thomas, K. Deka, P. Raviteja, and S. Sharma, "Convolutional Sparse Coding Based Channel Estimation for OTFS-SCMA in Uplink," *IEEE Transactions on Communications*, vol. 70, no. 8, pp. 5241–5257, 2022.
- [30] K. Deka, A. Thomas, and S. Sharma, "OTFS-SCMA: A Code-Domain NOMA Approach for Orthogonal Time Frequency Space Modulation," *IEEE Transactions on Communications*, vol. 69, no. 8, pp. 5043–5058, 2021.

- [31] H. Wen, W. Yuan, Z. Liu, and S. Li, "OTFS-SCMA: A Downlink NOMA Scheme for Massive Connectivity in High Mobility Channels," *IEEE Transactions on Wireless Communications*, vol. 22, no. 9, pp. 5770–5784, 2023.
- [32] J. Sun, Z. Wang, and Q. Huang, "An Orthogonal Time Frequency Space Direct Sequence Modulation Scheme," in *2021 IEEE International Conference on Communications Workshops (ICC Workshops)*, 2021, pp. 1–6.
- [33] Y. Cao, Z. Qiu, and H. Long, "A Sequence Spread Modulation Scheme Based on Orthogonal Time Frequency Space," in *2023 IEEE 97th Vehicular Technology Conference (VTC2023-Spring)*, 2023, pp. 1–5.
- [34] H. Wen, W. Yuan, and S. Li, "Downlink OTFS Non-Orthogonal Multiple Access Receiver Design based on Cross-Domain Detection," in *2022 IEEE International Conference on Communications Workshops (ICC Workshops)*, 2022, pp. 928–933.
- [35] Y. Xiong, F. Liu, Y. Cui, W. Yuan, T. X. Han, and G. Caire, "On the Fundamental Tradeoff of Integrated Sensing and Communications Under Gaussian Channels," *IEEE Transactions on Information Theory*, vol. 69, no. 9, pp. 5723–5751, 2023.
- [36] H. Hawkins, C. Xu, L.-L. Yang, and L. Hanzo, "IM-OFDM ISAC Outperforms OFDM ISAC by Combining Multiple Sensing Observations," *IEEE Open Journal of Vehicular Technology*, vol. 5, pp. 312–329, 2024.
- [37] C. Xu, L. Xiang, J. An, C. Dong, S. Sugiura, R. G. Maunder, L.-L. Yang, and L. Hanzo, "OTFS-Aided RIS-Assisted SAGIN Systems Outperform Their OFDM Counterparts in Doubly Selective High-Doppler Scenarios," *IEEE Internet of Things Journal*, vol. 10, no. 1, pp. 682–703, 2023.
- [38] L. Gaudio, M. Kobayashi, B. Bissinger, and G. Caire, "Performance Analysis of Joint Radar and Communication using OFDM and OTFS," in *2019 IEEE International Conference on Communications Workshops (ICC Workshops)*, 2019, pp. 1–6.
- [39] J. Shi, X. Hu, Z. Tie, X. Chen, W. Liang, and Z. Li, "Reliability performance analysis for OTFS modulation based integrated sensing and communication," *Digital Signal Processing*, vol. 144, p. 104280, 2024. [Online]. Available: <https://www.sciencedirect.com/science/article/pii/S1051200423003755>
- [40] L. Xiang, Y. Liu, C. Xu, R. G. Maunder, L.-L. Yang, and L. Hanzo, "Iterative Receiver Design for Polar-Coded SCMA Systems," *IEEE Transactions on Communications*, vol. 69, no. 7, pp. 4235–4246, 2021.
- [41] L. Li, Z. Ma, P. Z. Fan, and L. Hanzo, "High-Dimensional Codebook Design for the SCMA Down Link," *IEEE Transactions on Vehicular Technology*, vol. 67, no. 10, pp. 10118–10122, 2018.
- [42] W. Yuan, N. Wu, C. Yan, Y. Li, X. Huang, and L. Hanzo, "A Low-Complexity Energy-Minimization-Based SCMA Detector and Its Convergence Analysis," *IEEE Transactions on Vehicular Technology*, vol. 67, no. 12, pp. 12398–12403, 2018.
- [43] Y. Liu, L. Xiang, R. G. Maunder, L.-L. Yang, and L. Hanzo, "Hybrid Iterative Detection and Decoding of Near-Instantaneously Adaptive Turbo-Coded Sparse Code Multiple Access," *IEEE Transactions on Vehicular Technology*, vol. 70, no. 5, pp. 4682–4692, 2021.



Hugo Hawkins (Graduate Student Member, IEEE) received his B.Eng. degree in Electrical and Electronic Engineering from the University of Southampton with First Class Honours in 2021. He is currently undertaking a PhD within the Next Generation Wireless Research Group at the University of Southampton. His research interests include integrated sensing and communication.



Chao Xu (S'09-M'14-SM'19) received the B.Eng. degree in telecommunications from the Beijing University of Posts and Telecommunications, Beijing, China, the B.Sc. (Eng.) degree (with First Class Hons.) in telecommunications from the Queen Mary, University of London, London, U.K., through a Sino-U.K. joint degree Program in 2008, and the M.Sc. degree (with distinction) in radio frequency communication systems and the Ph.D. degree in wireless communications from the University of Southampton, Southampton, U.K.,

in 2009 and 2015, respectively. He is currently a Senior Lecturer with Next Generation Wireless Research Group, University of Southampton. His research interests include index modulation, reconfigurable intelligent surfaces, noncoherent detection, and turbo detection. He was recipient of the Best M.Sc. Student in Broadband and Mobile Communication Networks by the IEEE Communications Society (United Kingdom and Republic of Ireland Chapter) in 2009. He was also the recipient of 2012 Chinese Government Award for Outstanding Self-Financed Student Abroad and 2017 Dean's Award, Faculty of Physical Sciences and Engineering, the University of Southampton. In 2023, he was awarded Marie Skłodowska-Curie Actions (MSCA) Global Postdoctoral Fellowships with the highest evaluation score of 100/100.



Lie-Liang Yang (Fellow, IEEE) is the professor of Wireless Communications in the School of Electronics and Computer Science at the University of Southampton, UK. He received his MEng and PhD degrees in communications and electronics from Northern (Beijing) Jiaotong University, Beijing, China in 1991 and 1997, respectively, and his BEng degree in communications engineering from Shanghai TieDao University, Shanghai, China in 1988. He has research interest in wireless communications, wireless networks and signal processing for wireless communications, as well as molecular communications and nano-networks. He has published 400+ research papers in journals and conference proceedings, authored/co-authored three books and also published several book chapters. The details about his research publications can be found at <https://www.ecs.soton.ac.uk/people/llyang>. He is a fellow of the IEEE, IET and AAIA, and was a distinguished lecturer of the IEEE VTS. He served as an associate editor to various journals, and is currently a senior editor to the IEEE Access and a subject editor to the Electronics Letters. He also acted different roles for organization of conferences.



Lajos Hanzo (Life Fellow, IEEE) Lajos Hanzo (FIEEE'04) received Honorary Doctorates from the Technical University of Budapest (2009) and Edinburgh University (2015). He is a Foreign Member of the Hungarian Science-Academy, Fellow of the Royal Academy of Engineering (FREng), of the IET, of EURASIP and holds the IEEE Eric Sumner Technical Field Award. For further details please see <http://www-mobile.ecs.soton.ac.uk>, https://en.wikipedia.org/wiki/Lajos_Hanzo